Performance Analysis of a Permanent Magnet Synchronous Motor with Dual Stator Windings

O. J. Tola[1*], E. S. Obe[2, 3], L. U. Anih[2]

[1]Electrical and Electronic Department, Federal University of Technology, Minna, Nigeria;
[2] Electrical Engineering Department, University of Nigeria, Nsukka, Nigeria;
[3] Electrical, Computer and Telecommunication Engineering Department, Botswana International University of Science and Technology, Palapye, Botswana

ABSTRACT: This paper presents the modelling and performance analysis of a line-start three-phase interior permanent magnet synchronous motor (IPMSM) with dual stator windings. The machine has two sets of windings, main and auxiliary windings. The main winding is connected to the supply while the auxiliary is connected to a balanced capacitor. The dynamic model equations are derived in the d-q rotor reference frame using the concept of winding function theory. The machine input impedance was construed from the steady-state equations, where the effects of capacitance on the performance of the motor were studied. An improved torque was obtained when a suitable capacitance was connected to the auxiliary winding. A point of good performance was established by enhancing its direct axis reactance and the quadrature axis reactance which depend on the size of the capacitor. It is shown that the new configuration has better performance characteristics when compared with those of the traditional configuration in terms of output power, torque density and efficiency.

KEYWORDS: Dual stator windings, Line-start IPMSM, Balanced capacitor, Dynamic model, Torque enhancement.

[Received Nov. 28, 2022; Revised April 28, 2023; Accepted July 13, 2023] Print ISSN: 0189-9546 | Online ISSN: 2437-2110

SYMBOLS, ABBREVIATIONS AND UNITS

V_q, V_d : q-d axis voltages; i_q, i_d : q-d axis currents;

λ_q, λ_d : q-d flux linkages; where the q and d are the quadrature axis and the direct axix respectively.

r_s :Stator phase resistance; θ_r : Rotor angular position (radians);
δ : is the load angle;
ε : is the assumed displacement angle between ABC winding and XYZ winding;

L_{mq}, L_{md} : Magnetizing inductance in q-axis and d-axis;

L_{ls} : Stator winding leakage inductance; L_q :q-axis synchronous inductance;

L_d : d-axis synchronous inductance; $r_{kq}^{'}$ $r_{kd}^{'}$: equivalent q-axis and d-axis damper winding resistance; $\lambda_{kq}^{'}$ $\lambda_{kd}^{'}$:equivalent q-axis and d-axis damper flux linkage; $L_{kq}^{'}$ $L_{kd}^{'}$: equivalent q-axis and d-axis damper inductance; $i_{kq}^{'}$, $i_{kd}^{'}$: equivalent q-axis and d-axis damper current; $i_m^{'}$ equivalent magnetizing current of permanent magnets; λ_m : Flux linkage due to permanent magnets; ϕ : Stator circumferential position (radians); $N_a(\phi)$, $N_b(\phi)$, $N_c(\phi)$: Winding function of stator phase a, b and c respectively; $N_x(\phi)$, $N_y(\phi)$, $N_z(\phi)$: Winding function of stator phase x, y and z respectively; L_{ss} : Stator inductance matrix; β: Ratio of the pole arc to the pole pitch; $g^1(\phi,\theta_r)$: Inverse air gap function; g_1 : Minimum air-gap length; g_2 : Maximum air gap length; PM: Permanent magnet and Nd-Fe-B is Neodymium-Iron-Boron.

*Corresponding author: omokhafe@futminna.edu.ng
doi: http://dx.doi.org/10.4314/njtd.v18i4.1472

I. INTRODUCTION

The dwindling global energy resources and strict efficiency regulations dictate the need for energy efficiency practices in industrial settings. The sector utilizes energy to run lighting, machinery and high voltage AC equipment. As electric motors account for a larger proportion of global industrial energy consumption, it become necessary to evolve strategies to minimize their consumption.

Because of the high level of technology involved and the advancements made in permanent magnet materials, PMSM research has received a great deal of interest. Due to its considerably better efficiency, power factor, power density, and superior heat transfer ability, the machine becomes a desirable alternative to induction motor in a number of applications (Łukasz *et al*., 2020, Mousalreza *et al*., 2021) Its efficiency is higher than that of asynchronous motors, except that its price is somewhat higher owing to the addition of permanent magnets.

Several researchers improved on the performance of induction and reluctance motors using dual stator winding. However, slight thought has been paid to PMSM except the works of (Chandrasekaran and Manigandan, 2011; Basak and Chakraborty, 2015; Ogunjuyigbe *et al*., 2017), Zhiwei Zhang, 2021; Nazanin *et al.*, 2021). Moreover, a portion of the research accomplishments on how to improve the performance of electrical machines with two stator winding connected with a balanced capacitor for synchronous reluctance machines were described in (Anih and Obe, 2009; Obe, 2010; Anih *et al*., 2015). In (Anih and Obe, 2009) the machine comprises two sets of winding, main and auxiliary winding with a rounded rotor. Although, the secondary windings of the machine were transposed and short-circuited, both (main and secondary) windings were connected in series configurations. The result shows the performance of the machine operating at half synchronous speed and torque.

In (Ogunjuyigbe *et al*., 2009) the authors proposed an SRM that used the conventional rotor and three-phase supplementary winding, connected with a capacitor for power factor enhancement. Line-start interior permanent magnet synchronous motor (LSIPMSM) is an efficient motor that runs with a static line voltage and frequency as it is in an induction machine. However, by comparison, the motor power factor is higher and low losses at steady state (Almeida *et al*., 2011). At steady state, LSIPMSM has a higher efficiency and better power factor than induction motor (Barbara-Anne et al., 2021), (Mutize and Wang, 2013). The LSIPMSM face some significant challenges such as synchronisation and magnets braking torque which are noticeable especially during starting. On synchronisation, the optimal design of LSIPMSM with interior magnets and cage winding has been a trade-off between these challenges (Aliabad et al., 2010; Hassanpour et al.,2011). In (Hassanpour et al.,2011), the authors investigated the properties of magnetising inductance of LSPMSM on the starting characteristics, using the magnetising inductance, average and pulsating torques values in asynchronous action. Analysis revealed an improved start-up when concerted with high magnetisation inductance and high synchronisation ability with a resultant lower magnetisation inductance.

In (Cintron-Rivera *et al*., 2012), the authors proposed a simplified characterization of permanent magnet synchronous machine which include the effects of saturation. The PMSM also gained its popularity everyday owing to the availability of permanent magnet (PM) materials of high energy density like Nd-Fe-B, Samarium Cobalt and Ferrite. Rahman and Osheiba (Rahman and Osheiba, 1990), presented the performance of a large power PMSM with Sm-Co5 and Nd-Fe-B magnets. They succeeded in finding an expression that takes into account both the performance and the buildup. However, a high power factor and over 94% full load efficiency were attained in a motor made of Nd-Fe-B PM material.

Generally, winding function theory(WFT) adopted in many of the studies of modelling and analysis of electric machine (Di Nardo *et al*., 2022; Ni *et al*., 2022) to analyse the inductances of the windings and is relatively useful. WFT, as a tool for calculating the mmf, considers the winding layout in the modelling of the electrical machine. The concept (Obe, 2010) was used for the calculation of machine inductances with only the winding layout and air-gap geometry.

In this paper, we will use the WFT procedures on a dual-winding LSPMSM to enhance the output power using capacitance current injection to improve power factor. This improved performance will reduce the energy consumption of the motor, which saves cost and increases the lifespan of the motor. The permanent magnet synchronous motor (PMSMs) exhibits a higher torque density and a higher efficiency in comparison to induction machines of similar size. This paper is sub-divided into four sections. The background of the study has been presented in section I. The model machine description and the simulation results of the dynamic and detail steady-state analysis is presented in section II. In addition, the results of steady-state analysis are discussed in detailed in section III. The paper's section IV contains the conclusion.

II. METHODS

The machine windings were modified to comfortably carry two three-phase stator winding sets- main (ABC) and auxiliary (XYZ). The sets of windings, wherein magnetic axes displaced by an arbitrary angle ($\mathcal{E}$), share equal magnetic space and having poles of similar number residing in the same stator slots. Consequently, the windings are electrically isolated but magnetically coupled. The load current is on ABC winding whereas the XYZ winding is linked to a balanced capacitor. Attachment of the capacitor to XYZ winding consistently advances the power factor and torque. The moving member is simple dumb-bell salient pole rotor. Figure 1 shows the machine connection diagram. While the stator winding is reconfigured to fit the two sets of windings, the design kept the permanent magnet (PM), squirrel cage bar, and rotor in place. The windings in the 36-slot stator are curly and double-layered, with q=3 slots per pole and phase. The parameters of the model machine are of 4 HP, 4- pole, 230V, 50Hz as in (Tola *et al.*, 2017; Tola *et al.*, 2022).

The voltage and flux linkage equations of the dual stator winding machine are expressed as:

$$\begin{cases} V_{ABCs} = R_{ABC} i_{ABCs} + \rho\lambda_{ABCs} \\ 0 = R_{XYZ} i_{XYZs} + \rho\lambda_{XYZs} + V_{CXYZs} \\ V_{dqr} = R_{dqr} i_{dqr} + \rho\lambda_{dqr} \end{cases} \quad (1)$$

The main and auxiliary windings are defined by the subscripts ABC and XYZ respectively, while the stator and rotor variables are denoted by subscripts s and r. The equivalent resistances for the ABC and XYZ windings are R_{ABC} and R_{XYZ}respectively. The flux linkage expressions are shown as;

$$\begin{cases} \lambda_{ABCs} = L_{ABC} i_{ABCs} + L_{ABCXYZ} i_{XYZs} + L_{1r} i_{dq} + \lambda_{PM} \\ \lambda_{XYZs} = L^T_{ABCXYZ} i_{ABCs} + L_{XYZ} i_{XYZs} + L_{2r} i_{dq} + \lambda_{PM} \\ \lambda_{dqr} = L^T_{1r} i_{ABCs} + L^T_{2r} i_{XYZs} + L_r i_{dqr} + \lambda_{PM} \end{cases} \quad (2)$$

The inductances are represented in matrix form as:

$$L_{SS} = \begin{bmatrix} L_{ABC} & L_{ABCXYZ} & L_{1r} \\ L_{ABCXYZ} & L_{XYZ} & L_{2r} \\ L_{1r} & L_{2r} & L_r \end{bmatrix} \quad (3)$$

$$L_{ABCXYZ} = L_{12} + L_{l12}$$

where λ_{PM} is the PM material flux, which is connected to the stator and the two-rotor damper winding, and L_{12} and L_{l12} are the mutual inductances and leakage inductances between the two windings, respectively. In view of the sinusoida distribution flux linkages, the PM flux linkages are defined as;

$$\lambda_{PM} = \begin{bmatrix} \lambda_{pmq} \\ \lambda_{pmd} \end{bmatrix} = \begin{bmatrix} \lambda_m \cos\theta_r \\ \lambda_m \sin\theta_r \end{bmatrix} \quad (4)$$

These corresponding inductance values are calculated using winding function expressed as:

$$L_{ij} = \mu_0 r L \int_0^{2\pi} g^{-1}(\phi, \theta_r) N_r(\phi, \theta_r) N_j(\phi, \theta_r) d\phi \quad (5)$$

In Eqn. (5), the average radius of the air gap is r, L is the machine stack length, μ_0 is the permeability of free space, $N_i(\phi)$ and $N_j(\phi)$ are winding function of the i^{th} and j^{th} winding respectively and g^{-1} is the inverse air gap function of the machine. The inverse air gap function can be expressed (Obe and Senjyu, 2006) as:

$$g^{-1}(\phi,\ \theta_r) = m + n\cos 2(\phi - \theta_r) \quad (6)$$

Where

$$\begin{cases} m = \frac{\beta}{g_1} + \frac{(1-\beta)}{g_2} \\ n = \frac{2}{\pi}\left(\frac{1}{g_1} - \frac{1}{g_2}\right)\sin(\pi\beta) \end{cases} \quad (7)$$

where g_1 and g_2 are the minimum and maximum air gap lengths respectively and β is the pole arc-to-pitch ratio. With sinusoidally distributed windings, the WF in (5), contain only fundamental components. Therefore the ABC and XYZ winding sets expressed (Tola *et al.*, 2017) can be shown as:

$$N_{ij}(\phi) = \frac{N_{ij}}{2}\cos(\phi - \alpha_{ij}) \quad (8)$$

$$N_{ij}(\phi) = \frac{N_{ij}}{2}\cos(\phi - \alpha_{ij} - \varepsilon_{ij}) \quad (9)$$

where, the number of turns per pole per phase is: $N_{ij} = N_{ji} = N$. Substitute (6) in (5)

$$L_{ij} = L_{ji} = \frac{N_i N_j \mu_0 r l}{4} \int_0^{2\pi} \cos(\phi)(m + n\cos 2(\phi - \theta_r))d\phi \quad (10)$$

By integrating (10) the self and mutual inductances of ABC and XYZ windings are expressed.

$$L_{ABCs} = \begin{bmatrix} L_{lA} + L_{AA0} - L_{AA1}\cos(2\theta_r) & -\frac{1}{2}L_{AA0} - L_{AA1}\cos\left(2\theta_r - \frac{2\pi}{3}\right) & -\frac{1}{2}L_{AA0} - L_{AA1}\cos\left(2\theta_r + \frac{2\pi}{3}\right) \\ -\frac{1}{2}L_{AA0} - L_{AA1}\cos\left(2\theta_r - \frac{2\pi}{3}\right) & L_{lB} + L_{AA0} - L_{AA1}\cos\left(2\theta_r + \frac{2\pi}{3}\right) & -\frac{1}{2}L_{AA0} - L_{AA1}\cos(2\theta_r) \\ -\frac{1}{2}L_{AA0} - L_{AA1}\cos\left(2\theta_r + \frac{2\pi}{3}\right) & -\frac{1}{2}L_{AA0} - L_{AA1}\cos(2\theta_r) & L_{lC} + L_{AA0} - L_{AA1}\cos\left(2\theta_r - + \frac{2\pi}{3}\right) \end{bmatrix} \quad (11)$$

$$L_{XYZs} = \begin{bmatrix} L_{lX} + L_{XX0} - L_{XX1}\cos(2\theta_r - \varepsilon) & -\frac{1}{2}L_{XX0} - L_{XX1}\cos\left(2\theta_r - 2\varepsilon - \frac{2\pi}{3}\right) & -\frac{1}{2}L_{XX0} - L_{XX1}\cos\left(2\theta_r - 2\varepsilon + \frac{2\pi}{3}\right) \\ -\frac{1}{2}L_{XX0} - L_{XX1}\cos\left(2\theta_r - 2\varepsilon - \frac{2\pi}{3}\right) & L_{lY} + L_{XX0} - L_{XX1}\cos\left(2\theta_r - \varepsilon + \frac{2\pi}{3}\right) & -\frac{1}{2}L_{XX0} - L_{XX1}\cos(2\theta_r - 2\varepsilon) \\ -\frac{1}{2}L_{XX0} - L_{XX1}\cos\left(2\theta_r - 2\varepsilon + \frac{2\pi}{3}\right), & -\frac{1}{2}L_{XX0} - L_{XX1}\cos(2\theta_r - 2\varepsilon), & L_{lZ} + L_{XX0} - L_{XX1}\cos\left(2\theta_r - \varepsilon - + \frac{2\pi}{3}\right) \end{bmatrix} \quad (12)$$

Likewise, the coupling inductance between ABC and XYZ windings are expressed as:

$$L_{12} = \begin{bmatrix} L_{AX0}\cos\varepsilon - L_{AX1}\cos(2\theta_r - \varepsilon) & L_{AX0}\cos\left(\varepsilon + \frac{2\pi}{3}\right) - L_{AX1}\cos\left(2\theta_r - \varepsilon - \frac{2\pi}{3}\right) & L_{AX0}\cos\left(\varepsilon - \frac{2\pi}{3}\right) - L_{AX1}\cos\left(2\theta_r - \varepsilon + \frac{2\pi}{3}\right) \\ L_{AX0}\cos\left(\varepsilon - \frac{2\pi}{3}\right) - L_{AX1}\cos\left(2\theta_r - \varepsilon + \frac{2\pi}{3}\right) & L_{AX0}\cos\left(\varepsilon + \frac{2\pi}{3}\right) - L_{AX1}\cos\left(2\theta_r - \varepsilon + \frac{2\pi}{3}\right) & L_{AX0}\cos\left(\varepsilon - \frac{2\pi}{3}\right) - L_{AX1}\cos(2\theta_r - \varepsilon) \\ L_{AX0}\cos\varepsilon - L_{AX1}\cos\left(2\theta_r - \varepsilon + \frac{2\pi}{3}\right) & L_{AX0}\cos\left(\varepsilon - \frac{2\pi}{3}\right) - L_{AX1}\cos(2\theta_r - \varepsilon) & L_{AX0}\cos\varepsilon - L_{AX1}\cos\left(2\theta_r - \varepsilon - \frac{2\pi}{3}\right) \end{bmatrix} \quad (13)$$

Also, the stator-rotor inductance terms are:

$$L_{1r} = \begin{bmatrix} L_{1q}\cos\theta_r & L_{1d}\sin\theta_r \\ L_{1q}\cos\left(\theta_r - \frac{2\pi}{3}\right) & L_{1d}\sin\left(\theta_r - \frac{2\pi}{3}\right) \\ L_{1q}\cos\left(\theta_r + \frac{2\pi}{3}\right) & L_{1d}\sin\left(\theta_r + \frac{2\pi}{3}\right) \end{bmatrix} \quad (14)$$

$$L_{2r} = \begin{bmatrix} L_{2q}\cos(\theta_r - \varepsilon) & L_{2d}\cos(\theta_r - \varepsilon) \\ L_{2q}\cos\left(\theta_r - \varepsilon - \frac{2\pi}{3}\right) & L_{2d}\sin\left(\theta_r - \varepsilon - \frac{2\pi}{3}\right) \\ L_{2q}\cos\left(\theta_r - \varepsilon + \frac{2\pi}{3}\right) & L_{2d}\sin\left(\theta_r - \varepsilon + \frac{2\pi}{3}\right) \end{bmatrix} \quad (15)$$

The voltage equations can be written with a referred parameter in rotor reference frame variable as:

$$\begin{cases} V_{q1}^r = r_1 i_{q1}^r + \omega_r \lambda_{d1}^r + \rho \lambda_{q1}^r \\ V_{d1}^r = r_1 i_{d1}^r - \omega_r \lambda_{q1}^r + \rho \lambda_{d1}^r \\ V'^r_{q2} = r_2'^r i'^r_{q2} + \omega_r \lambda'^r_{d2} + \rho \lambda'^r_{q2} + V_{Cq}'^r \\ V'^r_{d2} = r_2'^r i'^r_{d2} - \omega_r \lambda'^r_{q2} + \rho \lambda'^r_{d2} + V_{Cd}'^r \\ V_{qr} = r_{kq} i_{qr} + \rho \lambda_{qr} = 0 \\ V_{dr} = r_{kd} i_{dr} + \rho \lambda_{dr} = 0 \end{cases} \quad (16)$$

Where

$$\begin{cases} \lambda_{q1}^r = L_{ls1} i_{q1}^r + L_{mq}\left(i_{q1}^r + i_{q2}^r + i_{kq}\right) \\ \lambda_{d1}^r = L_{ls1} i_{d1}^r + L_{md}(i_{d1}^r + i_{d2}^r + i_{kd}) + \lambda_{PM} \\ \lambda_{q2}^r = L_{ls2} i_{q2}^r + L_{mq}\left(i_{q1}^r + i_{q2}^r + i_{kq}\right) \\ \lambda_{d2}^r = L_{ls2} i_{d2}^r + L_{md}(i_{d1}^r + i_{d2}^r + i_{kd}) + \lambda_{PM} \\ \lambda_{kq} = L'_{lkq} i_{kq} + L_{mq}\left(i_{q1} + i_{q2} + i_{kq}\right) \\ \lambda_{kd} = L'_{lkd} i_{kd} + L_{md}(i_{d1} + i_{d2} + i_{kd}) + \lambda_{PM} \end{cases} \quad (17)$$

Moreover, the voltage of the capacitor in the rotor reference frame is expressed as:

$$\begin{cases} \rho V_{Cd}'^r = \frac{i_d'^r}{C} + \omega_r V_{Cq}'^r \\ \rho V_{Cq}'^r = \frac{i_q'^r}{C} - \omega_r V_{Cd}'^r \end{cases} \quad (18)$$

The expression for electromagnetic torque is given by:

$$T_e = \frac{3n}{4}\left[\left(\lambda_{d1}^r i_{q1}^r - \lambda_{q1}^r i_{d1}^r\right) + \left(\lambda_{d2}^r i_{q2}^r - \lambda_{q2}^r i_{d2}^r\right)\right] \quad (19)$$

where n is the number of poles of the machine.

Substituting flux linkage equations (17) in (19), we have:

$$T_e = \frac{3n}{4}[T_1 + T_2 + T_3 + T_4 + T_5] \quad (20)$$

Where

$$\begin{cases} T_1 = \left(L_{d1} - L_{q1}\right) i_{d1}^r i_{q1}^r \\ T_2 = \left(L_{d2} - L_{q2}\right) i_{d2}^r i_{q2}^r \\ T_3 = \left(i_{q1}^r - i_{q2}^r\right) \lambda_{PM} \\ T_4 = \left(L_{md} - L_{mq}\right) i_{d1}^r i_{q2}^r + \left(L_{md} - L_{mq}\right) i_{11}^r i_{d2}^r \\ T_5 = \left(L_{1d} i_{kd} i_{q1}^r - L_{1q} i_{kq} i_{d1}^r\right) + \left(L_{2d} i_{kd} i_{q2}^r - L_{2q} i_{kq} i_{d2}^r\right) \end{cases} \quad (21)$$

In (20), T_1 represent reluctance torque by abc winding, T_2 also represent reluctance torque by xyz winding. T_3 is the torque owing to PM material excitation. T_4 depicts torque expression owing to interaction between abc and xyz winding. Finally, T_5 depicts torque owing to interaction between abc, xyz and cage windings.

The use of exponential fits of a known machine accounted for saturation effects. The machine parameters which were expressed as a function of flux linkages were used to analyze the inductances in place of constant inductance values. The expressions given by (Ojo and cox, 1996) are:

$$\begin{cases} L_q = 0.492 e^{\left(-0.87 i_s + 0.23 i_s^2 - 0.03 i_s^3\right)} \\ L_d = 0.221 e^{\left(-0.91 i_s + 0.21 i_s^2 - 0.025 i_s^3\right)} \end{cases} \quad (22)$$

Magnetic flux due to PM material is assumed to be unchanged by saturation effects, whereas a change in reluctance due to parameter variations caused by saturation effects. The magnetic flux caused by PM and the subsequent impacts of saturation-related parameter fluctuations were used to analyze the torque production.

A. Dynamic simulation

Eqns. (16 - 22) represent the machine's dynamic model. When the machine was fully loaded, the starting performance is shown in Figure 3, and the rotor speed fluctuated for just 0.35 seconds at a speed of 314 rad/s. Compared to a conventional machine, the machine stabilizes at a load of 20 Nm at 6 seconds in 0.9 seconds. The rotor's speed, however, was equal to synchronous at the synchronization point. Figure 4 displays the electromagnetic torque in (21) along with other torque components. It has been noted that the induction torque, shown in Figure 4(e), provides the greatest torque input.

B. Steady-state Analysis

The performance of the machine with respect to the steady state was examined under the condition that time-varying terms of Eqn. (16) are set to zero, assuming the cage current is negligible and using the rotor reference frame.

$$\begin{cases} V_{q1}^r = r_1 I_{q1}^r + \omega_r \lambda_{d1}^r \\ V_{d1}^r = r_1 I_{d1}^r - \omega_r \lambda_{q1}^r \\ V_{q2}^r = r_2 I_{q2}^r + \omega_r \lambda_{d2}^r + V_{cq} \\ V_{d2}^r = r_2 I_{d2}^r - \omega_r \lambda_{q2}^r + V_{cd} \end{cases} \quad (23)$$

Considering the general expression for ABC and XYZ winding as [8]:

$$\begin{cases} F_a e^{-j\delta} = F_{q1}^r - j F_{d1}^r \\ F_x e^{-j(\delta-\varepsilon)} = F_{q2}^r - j F_{d2}^r \end{cases} \quad (24)$$

Where F may be flux linkage, current or voltage, δ is the load angle and ε is the assumed displacement angle between ABC winding and XYZ winding.

Although, ABC winding has no supply voltage, ABC winding voltage is:

$$\begin{cases} V_{q1}^r = V \cos\delta \\ V_{d1}^r = -V \sin\delta \end{cases} \quad (25)$$

The phasor form of the steady-state voltage equations can be expressed by substituting Eqn. (25) in (23) and simplifying with (24) and gives:

$$\begin{cases} V_a = (R_1 + jX_A) I_A + jX_{mq}(I_A - I_X) e^{j\varepsilon} + U_1 \\ 0 = (R_2 + jX_B) I_X + jX_{mq}(I_A - I_X) e^{j\varepsilon} + U_2 \end{cases} \quad (26)$$

Where

$$\begin{cases} U_1 = U_A + E_{PM} e^{j\delta} \\ X_A = X_L + X_{mq} e^{j\delta} \\ X_B = U_A - X_C \\ U_2 = U_B + E_{PM} e^{j(\delta-\varepsilon)} \end{cases} \quad (27)$$

$\left(X_{l1} + X_{mq}\right) = \left(X_{l2} + X_{mq}\right) = (X_{l1} + X_{md}) = (X_{l2} + X_{md}) = X_L$

$$\begin{cases} U_A = \left(\left(X_{md} - X_{mq}\right) I_{d2}\right) e^{j\delta} \\ U_B = \left(\left(X_{md} - X_{mq}\right) I_{d1}\right) e^{j(\delta-\varepsilon)} \end{cases}$$

E_{PM} is the permanent magnet voltage.

$$\begin{cases} I_a e^{-j\delta} = I_{q1}^r - j I_{d1}^r \\ I_X e^{-j(\delta-\varepsilon)} = I_{q2}^r - j I_{d2}^r \end{cases} \quad (28)$$

Eqns. (26) can be used to draw the steady-state equivalent circuit of the machine as depicted in Figure 2.

From Figure 2, the input impedance of the machine, neglecting resistances given by:

$$Z_{in} = \frac{V_a}{I_A} = \frac{(V_{q1} - jV_{d1})e^{j\delta}}{(I_{q1} - jI_{d1})e^{j\delta}} = \frac{V_s e^{j\delta}}{\frac{V_s(X_C - X_q)\sin\delta}{X_{mq}^2 - X_q^2 + X_C X_q} + \frac{(E_{PM}X_C - E_{PM}X_d + E_{PM}X_{md} - V_s X_C \cos\delta + V_s X_d \cos\delta)j}{X_{md}^2 - X_d^2 + X_C X_d}} \quad (29)$$

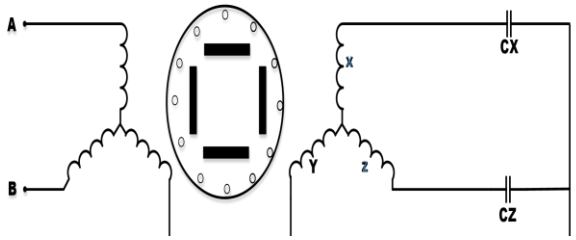

Figure 1: Physical arrangement of the model machine.

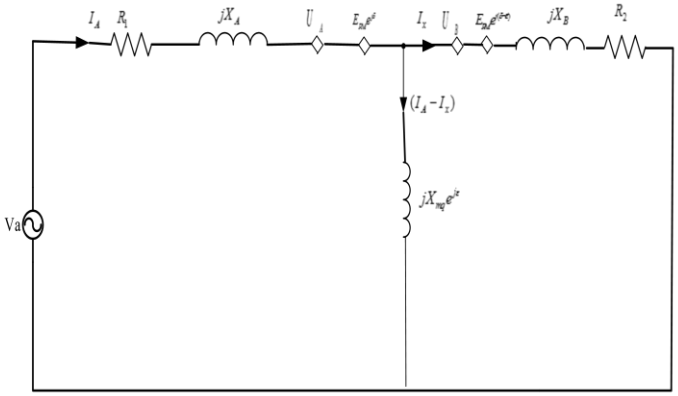

Figure 2: Steady-state equivalent circuit of the model machine.

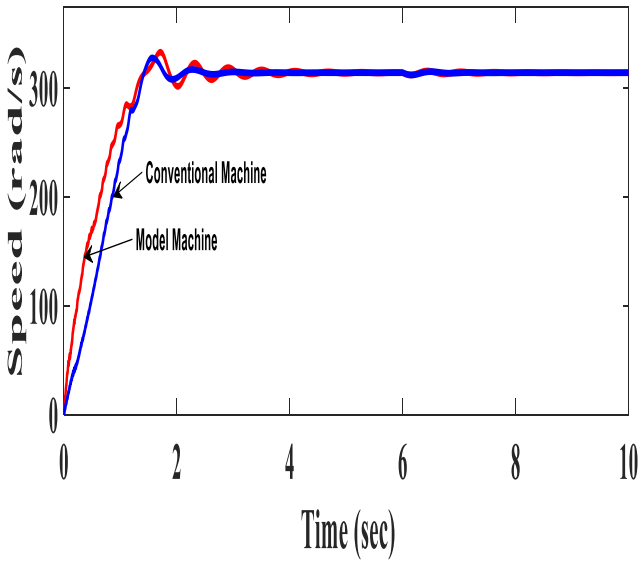

Figure 3: Rotor speed during starting of the Model and the Conventional Machine.

The capacitor value of the machine selected is by considering (29) for the following conditions.

When the rotor coincides with the d-axis, $\delta = 0$ then d-axis reactance is given as:

$$X_d = -\frac{jV_s(X_{md}^2 - X_d^2 + X_C X_d)}{V_s X_d - V_s X_C + E_{PM}X_C - E_{PM}X_d + E_{PM}X_{md}} \quad (30)$$

when the rotor coincides with the q-axis, $\delta = \frac{\pi}{2}$ then q-axis reactance is given as:

$$X_q = \frac{jV_s}{\frac{j(E_{PM}X_C - E_{PM}X_d + E_{PM}X_{md})}{X_{md}^2 - X_d^2 + X_C X_d} + \frac{V_s(X_C - X_q)}{X_{mq}^2 - X_q^2 + X_C X_q}} \quad (31)$$

The expression for electromagnetic torque developed in a steady state of the machine is:

$$T_e = \frac{3n}{4\omega}\left[\frac{V_s \sin\delta(E_{PM}X_C - E_{PM}X_d + E_{PM}X_{md} - V_s X_C \cos\delta + V_s X_d \cos\delta)}{X_{md}^2 + X_d(X_C - X_d)} + \frac{1}{2}\left(\frac{V_s^2 \sin 2\delta(X_C - X_q)}{X_{mq}^2 + X_q(X_C - X_q)}\right)\right] \quad (32)$$

The power factor obtained of the model machine by considering the real and the imaginary part of the input impedance as expressed in (Anih *et al.*, 2015):

$$\cos\varphi = \frac{realZ_{in}}{\sqrt{(realZ_{in})^2 + (imgZ_{in})^2}} \quad (33)$$

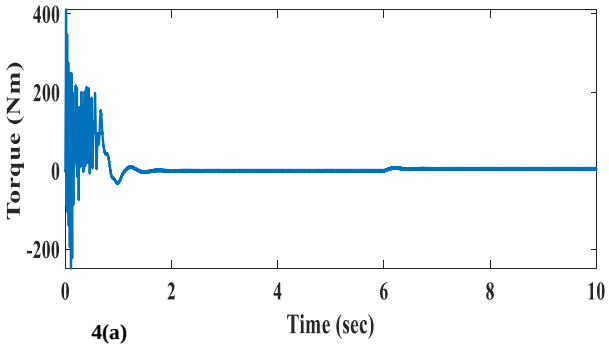

4(a)

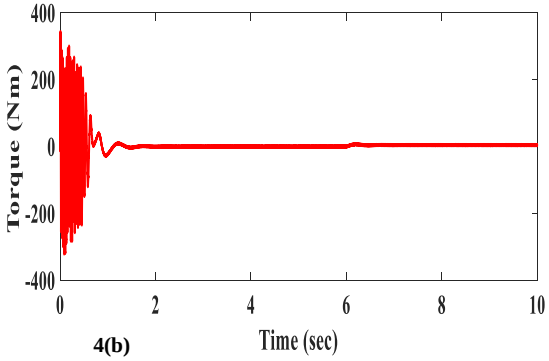

4(b)

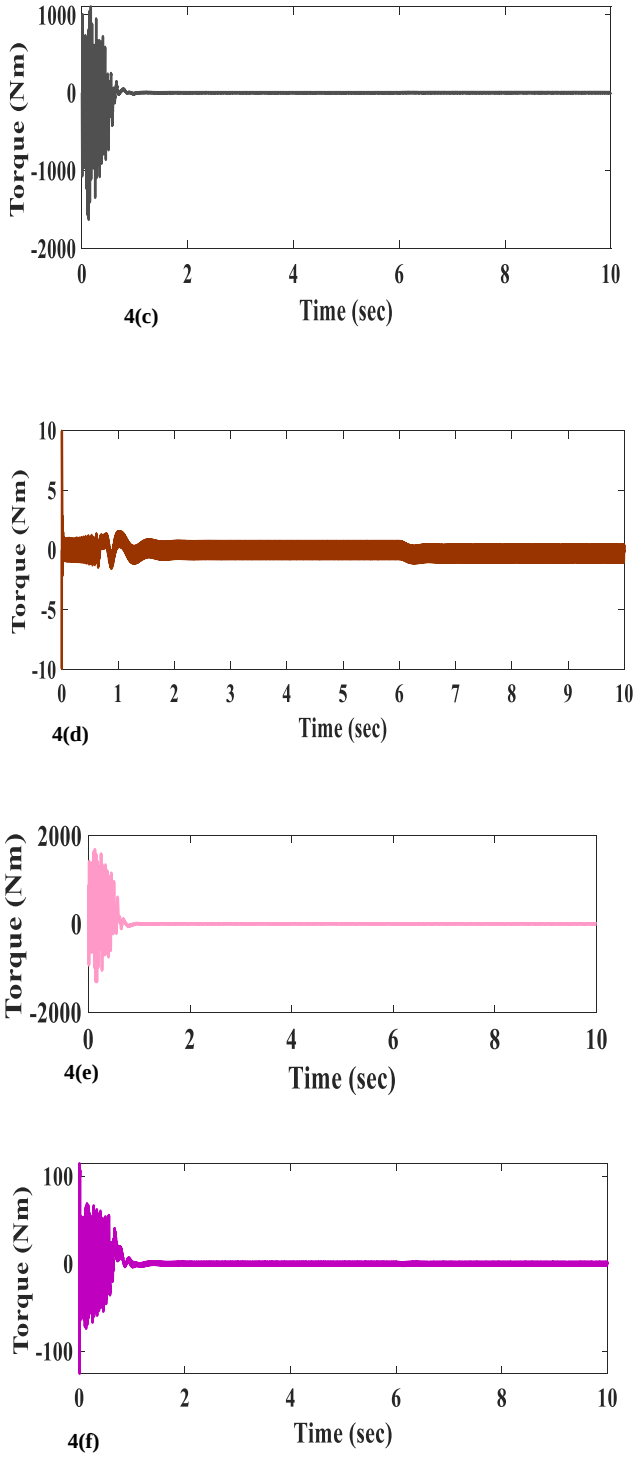

Figure 4: Torque developed by of the model machine (a) Electromagnetic torque, (4b) Excitation torque due to PM, (4c) Reluctance torque due to ABC windings, (4d) Reluctance torque due to XYZ windings, (4e) Induction torque due to dual windings and (4f) Torque due to interaction between (dual and Cage) windings.

III. RESULTS AND DISCUSSION

The choice of capacitor value is made possible, by the plot of equations (29) and (30) with respect to the capacitive reactance as shown in Figure 5. Note that the plots include the winding resistance to avoid the singularities arising from plotting the expression of X_d and X_q directly. The plots of direct and quadrature axes reactance and the ratio $\frac{X_q}{X_d}$ against capacitor are shown in Figure 5. It can be readily shown from the graph that the resonant peak occurs at $X_C = 40\Omega$.

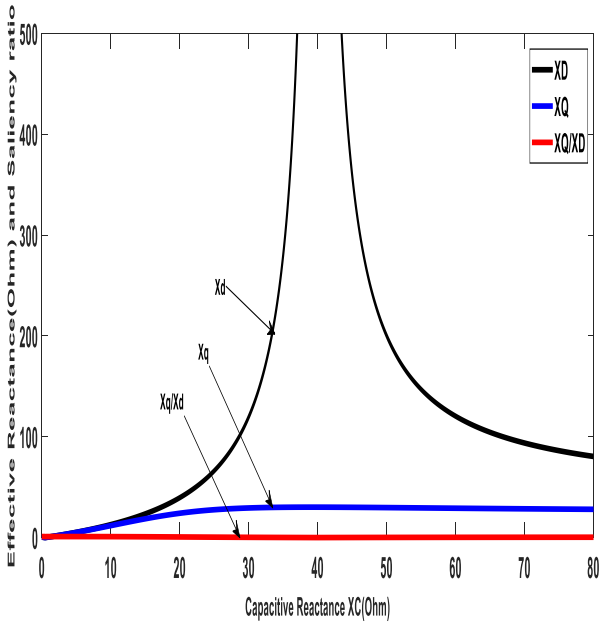

Figure 5: Variation of the Effective Reactance with Capacitive Reactance.

A. Performance Analysis

1) Performance using Impedance and Current Loci

In (Anih *et al.*, 2015) , there is a thorough discussion of the analysis using the circle diagram of a salient pole machine. The issue of connecting the impedance and capacitive reactance values of the electric machine has a visual solution in the form of the circle diagram. To analyze the performance in terms of torque, power factor, and stator current losses, the information from the circle diagrams was used.

Selective capacitance values from Figure 5 can be used to analyze the impedance and current loci, including values for open circuit ($X_C = \infty$) and short-circuit ($X_C = 0$). A family of circles with radii $\left[0, \frac{1}{2}(X_q + X_d)\right]$ and centre $\left[\frac{1}{2}(X_q + X_d)\right]$were produced by the locus of (29) when the load angle varied from 0 to 2π for different capacitor values, as illustrated in Figures 10a and 10b. X_d and X_q depend on the capacitor value. It is important to note that a machine's output power corresponds to the impedance circle's diameter. Figure 10b illustrates the current locus, which is a circle and is the inverse of the impedance locus.

2) Verification of Power Loss using Transient Parameters Extraction

In order to ascertain and confirm the machine power losses with regard to load angle, a dynamic simulation of the stator current main and auxiliary winding as well as the cage rotor

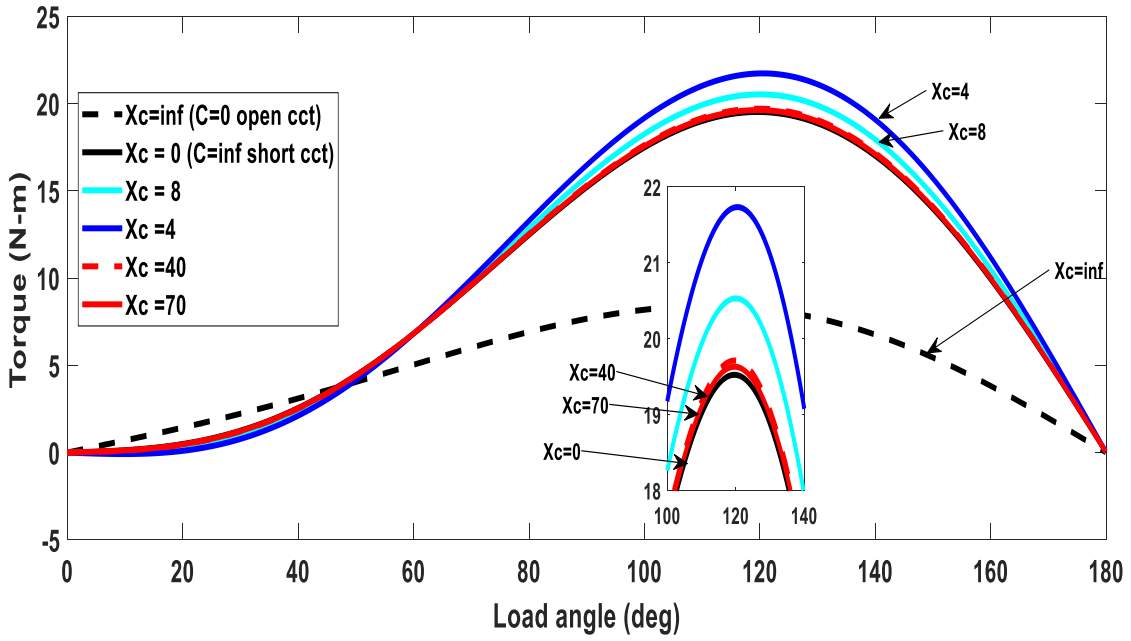

Figure 6: Torque - angle plot of the machine.

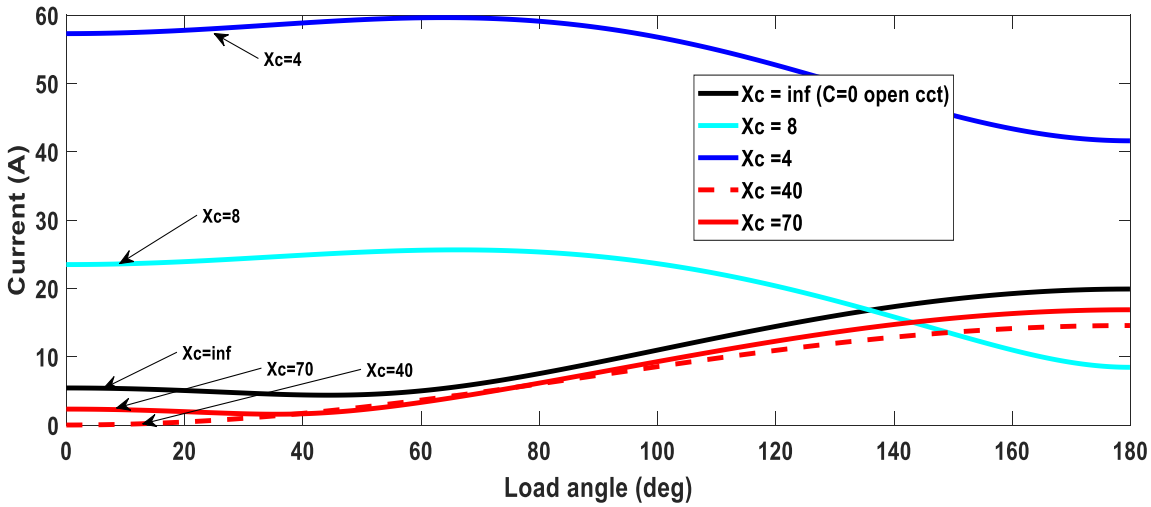

Figure 7: Main winding current - angle plot of the machine.

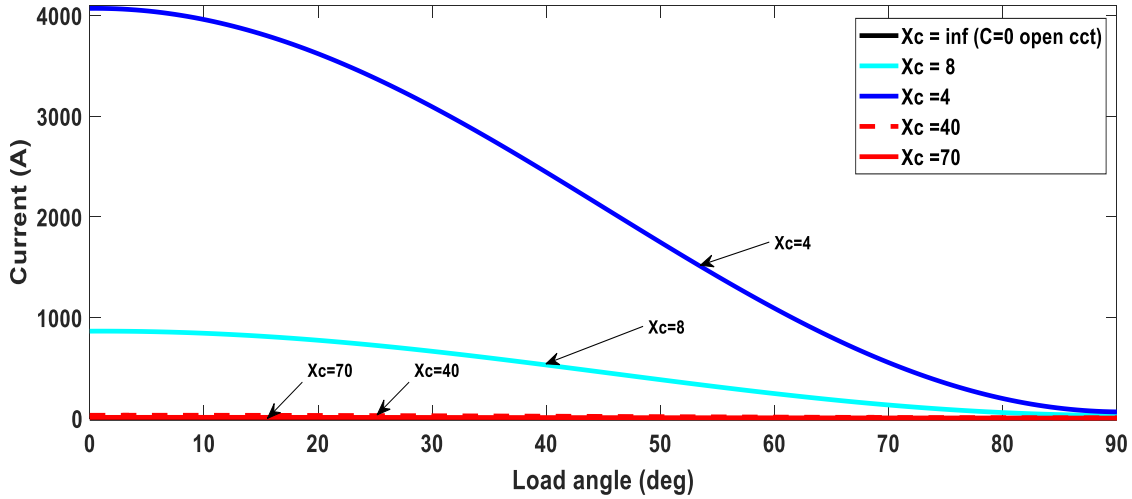

Figure 8: Auxiliary winding current - angle plot of the machine.

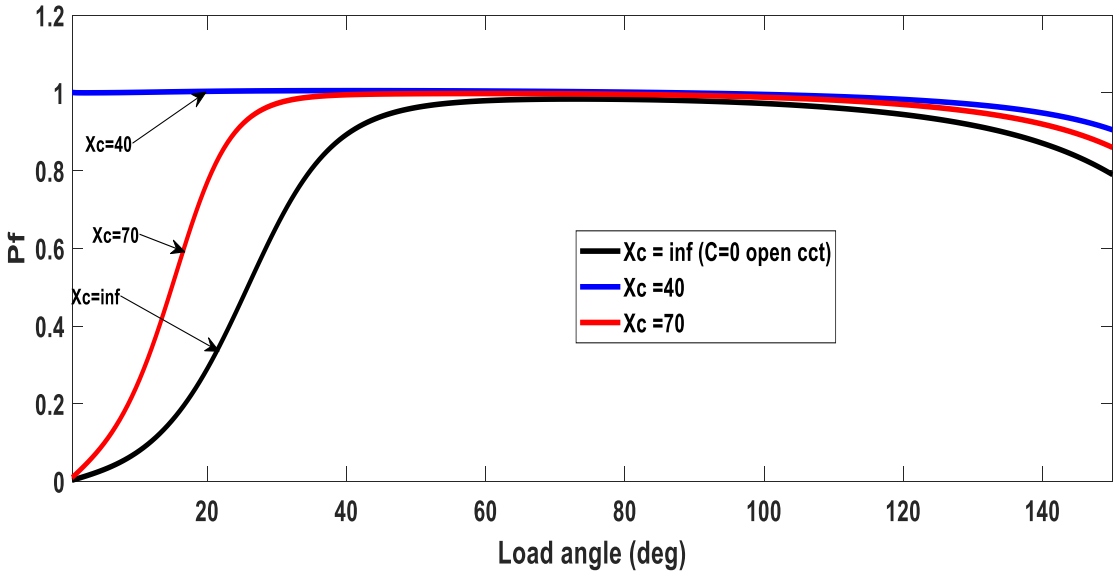

Figure 9: The power factor - angle plot of the machine.

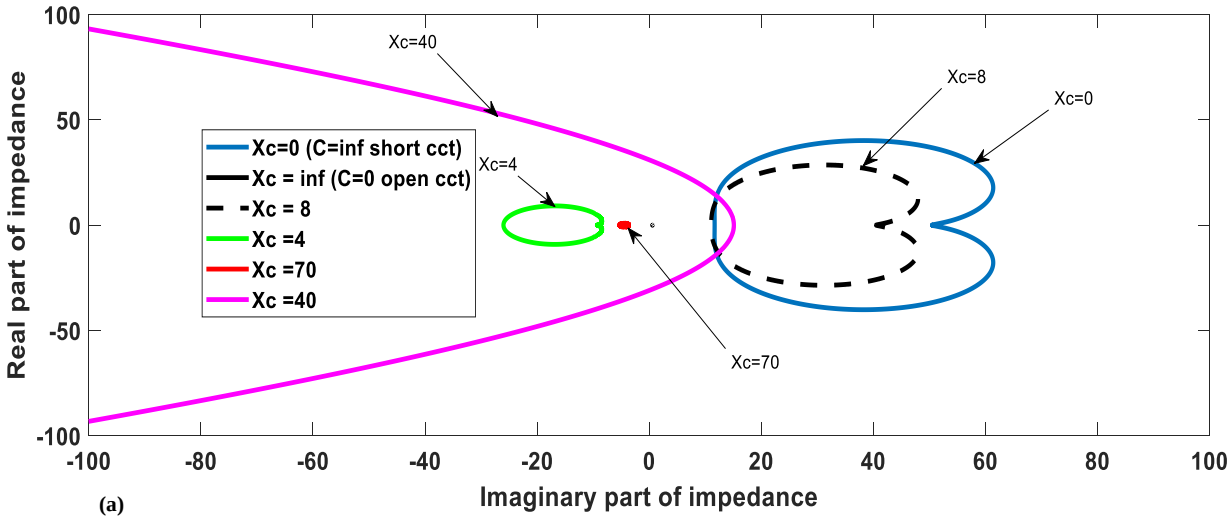

(a)

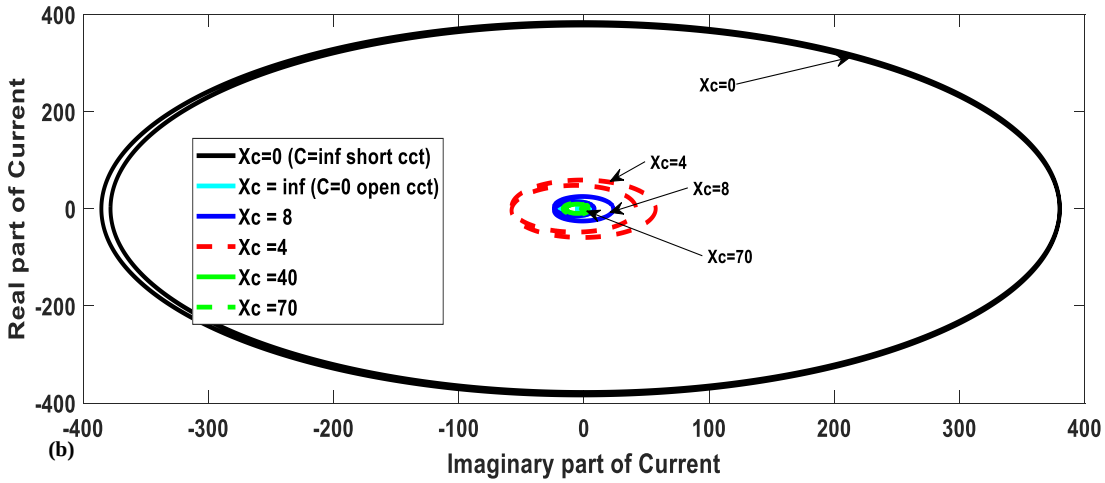

(b)

Figure 10: The Locus Plot of the model machine (a) Impedance (b) Current.

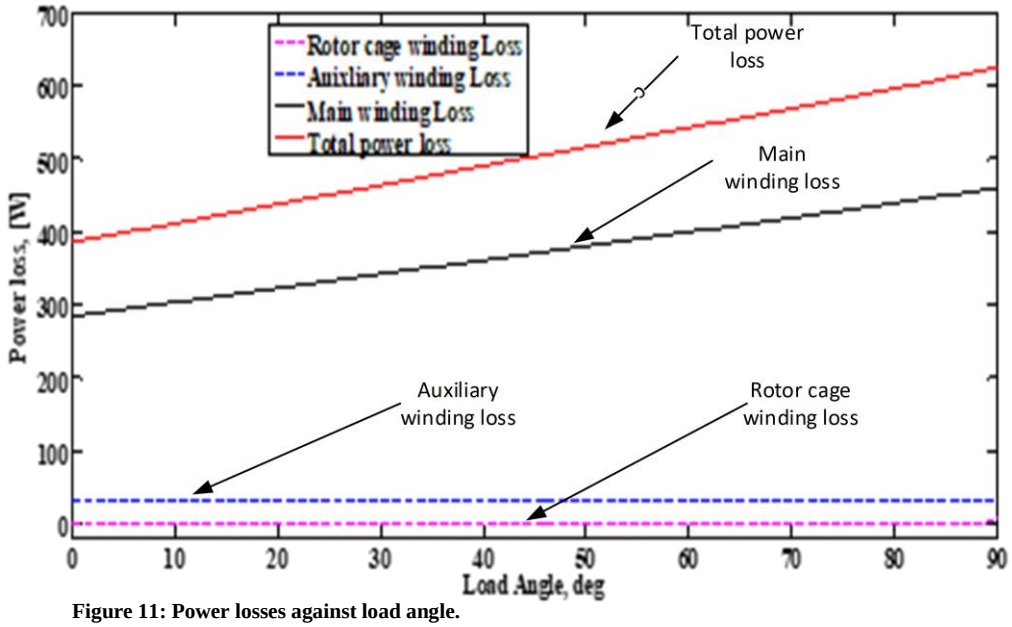

Figure 11: Power losses against load angle.

current with a balanced 40μF capacitor connected across the auxiliary is analysed.

The torque-angle relationship obtained for short-circuiting, open-circuit, and different values of X_C is shown in Figure 6, where the maximum torque of the machine is seen. The largest maximum torque value is provided by $X_C = 40$, but the current drawn is intolerably high and could endanger the stator winding insulation, as seen in Figures 7 and 8. The torque values for $X_C = 80$, $X_C = 40$, $X_C = 70$ and $X_C = \infty$, are large, however the current against these values is lower than that of of $X_C = 40$. However, the torque values for $X_C = 80$, $X_C = 40$, and $X_C = 70$, are all higher than those for the conventional machine. An observed power factor in Figure 9 that is close to unity is $X_C = 40$. The machine's total ohmic losses are depicted in Figure 11. In comparison to the machine's rated power (2.941 kW), the overall losses brought on by the stator winding and rotor cage winding are frequently negligible. The machine's output power and the overall losses exhibit fair agreement.

IV. CONCLUSION

The possibility of using dual winding together with capacitance current injection to improve the torque, and power factor, which tend to improve the overall performance characteristics of the LSIPMSM with dual stator windings as validated in this study. The development of the mathematical model for transient and steady-state analysis of the model machine as well as the equivalent circuit as presented. The equations suggest that the output torque is high with the highest torque contribution from the induction torque. The equivalent circuit and the circle diagram were used to analyse the selection of the optimal capacitor value. Moreover, the performance characteristics of the dual-winding line-start interior permanent magnet synchronous motor deduced from the input impedance under the condition that rotor coincides with d-axis, δ=0 and the rotor coincides with q-axis, $\delta = \frac{\pi}{2}$. Four capacitance points as a point of good performance established to correspond to $X_C = 40$, $X_C = 80$, $X_C = 40$, $X_C = 70$. From the results presented, the model machine provides enhanced torque and a good power factor by connecting a capacitive reactance $X_C = 40$ to the auxiliary winding. The appropriate capacitor value selection revealed the potential application of the machine as a power factor near unity is observed.

AUTHOR CONTRIBUTIONS

O. J. Tola: Wrote the paper, designed the model and analyzed the results. **E. S. Obe:** Contributed to the study idea and provided scientific content to the manuscript preparation and revision. **L. U. Anih:** Helped in analyzing the results, suggested modifications to the models and approved the final version of the manuscript.

REFERENCES

Aliabad, A.D.; Mirsalim, M. and Ershad, N.F. (2010). Line-Start Permanent-Magnet Motors: Significant Improvements in Starting Torque, Synchronization, and Steady-State Performance. *IEEE Transactions on Magnetics*, 46(12).

Almeida, A.T.; Ferreira, F.J. and Fong, J.A.C. (2011). Standards for Efficiency of Electric Motors. *IEEE Industry Applications Magazine*, 17(1), pp. 12–19. doi:10.1109/MIAS.2010.939427.

Anih, L.U. and Obe, E.S. (2009). Performance analysis of a composite dual-winding reluctance machine. *Energy Conversion and Management*, 50, pp. 3056–3062.

Anih, L.U.; Obe, E.S. and Abonyi, S.E. (2015). Modelling and performance of a hybrid synchronous reluctance machine with adjustable X d / X q ratio. *IET Electric Power Applications*, pp. 171–182. doi:10.1049/iet-epa.2014.0149.

Barbara-Anne K.; Amin, M. and Kahourzade, S. (2021). Line-Start Permanent-Magnet Synchronous Motor versus Induction Motor: Technical, Environmental and

Economical Considerations., *IEEE 12th Energy Conversion Congress & Exposition - Asia (ECCE-Asia)*. Singapore, Singapore: IEEE. doi:10.1109/ECCE-Asia49820.2021.9479424.

Basak, S. and Chakraborty, C. (2015). Dual stator winding induction machine: Problems, progress, and future scope. *IEEE Transactions on Industrial Electronics*, 62(7), pp. 4641–4652. doi:10.1109/TIE.2015.2409800.

Chandrasekaran, V. and Manigandan, T. (2011). Design and Effective Operation of Double Winding Synchronous Reluctance Motor, International Journal of Computer and Electrical Engineering, Vol 3(3). doi: 10.7763/IJCEE.2011.V3.356.

Cintron-Rivera, J. G.; Babel, A. and Strangas, E. (2012). A simplified characterization method including saturation effects for permanent magnet Machines. *Proceedings - 2012 20th International Conference on Electrical Machines, ICEM 2012*, pp. 837–843. doi:10.1109/ICElMach.2012.6349974.

Hassanpour I., A. and Vaez-Zadeh, S. (2011). Effects of Magnetizing Inductance on Start-Up and Synchronization of Line-Start Permanent-Magnet Synchronous Motors. *IEEE Transactions on Magnetics*, 47(4), pp. 823–829. doi:10.1109/TMAG.2010.2091651.

Łukasz, K. N.; Pawełoszek, K. and Menach, Y. Le (2020). Optimization of Low-Power Line-Start PM Motor Using Gray Wolf Metaheuristic Algorithm. *energies*, 13(1186). doi:10.3390/en13051186.

Mousalreza, F. P.; Wen, L.; Soong, N.B. and Wang, R.-J. (2021). Design and Optimisation Techniques in Performance Improvement of Line-Start Permanent Magnet Synchronous Motors: A Review. *IEEE Transaction on Magnetic* 57(9). doi:10.1109/TMAG.2021.3098392,.

Mutize, C. and Wang, R.-J. (2013). Performance Comparison of Induction Motor and Line-start PM motor for Cooling Fan Applications. *Proceedings of SAUPEC*.

Di Nardo; Gallicchio, G.; Palmieri, M. and Marfoli, A. (2022). High Speed Permanent Magnet Assisted Synchronous Reluctance Machine - Part II: Performance Boundaries. *IEEE Transactions on Energy Conversion*, 8969(c). doi:10.1109/TEC.2022.3176383.

Nazanin, A.; Jafar, M.; Mehrdad, A. and M. H. Zamani (2021). Improving Transient Stability of Dual Stator-Winding Induction Generator Based-Wind farms By Slip Frequency Control. *IEEE Journal of Emerging and Selected Topics in Power Electronics*, pp. 1–1. doi:10.1109/JESTPE.2021.3059967.

Ni Sijie, G. B.; Raphaël, R.; Bertrand, C. and Jean ,L. (2022). Damper Winding for Noise and Vibration Reduction of a Permanent Magnet Synchronous Machine. *Sensors*, 22(7). doi:10.3390/s22072738.

Obe, E.. and Senjyu, T. (2006). Analysis of a polyphase synchronous reluctance motor with two identical stator windings. *Electric Power System Research*, 76, pp. 515–524. doi:10.1016/j.epsr.2005.07.004.

Obe, E.S. (2010). Steady-state performance of a line-start synchronous reluctance motor with capacitive assistance. *Electric Power Systems Research*, 80(10), pp. 1240–1246. doi:10.1016/j.epsr.2010.04.004.

Ogunjuyigbe, A.S.O.; Obe, E. S. and Nicolae, D. V.. (2009). Synchronous Reluctance Machine with Magnetically-Coupled, Double Three-Phase Windings. *Electric Drives' Joint Symposium, ELECTROMOTION*. Lille, France, pp. 1–3.

Ogunjuyigbe, A.S.O.; Jimoh, A.A. and Ayodele, T.R. (2017). Dynamic and transient behaviour of a line start , capacitance compensated synchronous reluctance machine. *Journal of Electrical Systems and Information Technology*, pp. 1–18. doi:10.1016/j.jesit.2016.12.012.

Ojo, O. and Cox, J. (1996). Investigation into the performance characteristics of an interior permanent magnet generator including saturation effects. *Industry Applications Conference, 1996. Thirty-First IAS Annual Meeting, IAS '96.* San Diego, CA, USA, USA: IEEE, pp. 533–540. doi:10.1109/IAS.1996.557084.

Rahman, M.A. and Osheiba, A.M. (1990). Performance of Large Line Start Permanent Magnet Synchronous Motors. *IEEE Transaction on Energy Conversion*, 5(1), pp. 211–217.

Tola, O. J. ; Obe, E. S.; Obe, C. T. and Anih, L. U. (2022). Finite Element Analysis of Dual Stator Winding Line Start Permanent Magnet Synchronous Motor, Przegląd Elektrotechniczny 2022 | R. 98, nr 4 | 47—52, doi:10.15199/48.2022.04.11.

Tola, O. J.; Obe, E.S. and Anih, L.U. (2017). Modeling and analysis of dual stator windings permanent magnet synchronous motor. *IEEE 3rd International Conference on Electro-Technology for National Development (NIGERCON)*. Owerri, Nigeria: IEEE, pp. 861–871. doi:10.1109/NIGERCON.2017.8281954.

Zhiwei Zhang (2021). A Robust Non-Permanent Magnet Five-Phase Synchronous Reluctance Traction Motor. *IEEE Transportation Electrification Conference & Expo (ITEC)*. Chicago, IL, USA: IEEE. doi:10.1109/ITEC51675.2021.9490116.